

General relativistic treatment of the thermal, magnetic and rotational evolution of isolated neutron stars with crustal magnetic fields

D. Page¹, U. Geppert², and T. Zannias³

¹ Instituto de Astronomía, UNAM, 04510 Mexico D.F., Mexico (page@astroscu.unam.mx)

² Astrophysikalisches Institut Potsdam, An der Sternwarte 16, 14482 Potsdam, Germany (urme@aip.de)

³ Instituto de Física y Matemáticas, Universidad Michoacana SNH, 58040 Morelia, México (zannias@ginette.ifm.umich.mx)

Received 23 March 2000 / Accepted 15 June 2000

Abstract. We investigate the thermal, magnetic and rotational evolution of isolated neutron stars assuming that the dipolar magnetic field is confined to the crust. Our treatment, for the first time, uses a fully general relativistic formalism not only for the thermal but also for the magnetic part, and includes partial general relativistic effects in the rotational part. Due to the fact that the combined evolution depends crucially upon the compactness of the star, three different equations of state have been employed in the calculations. In the absence of general relativistic effects, while upon increasing compactness a decrease of the crust thickness takes place leading into an accelerating field decay, the inclusion of general relativistic effects intend to “decelerate this acceleration”. As a consequence we find that, within the crustal field hypothesis, a given equation of state is compatible with the observed distribution of pulsar periods P and period derivative \dot{P} provided the initial field strength and current location as well as the magnitude of the impurity content are appropriately constrained.

Finally, we access the flexibility of the soft, medium and stiff classes of equations of state as candidates in describing the state of the matter in the neutron star interiors. The comparison of our model calculations with observations, together with the consideration of independent information about neutron star evolution, suggests that a not too soft equation of state describes neutron star interiors and its cooling proceeds along the ‘standard’ scenario.

Key words: stars: neutron – stars: pulsars: general – stars: magnetic fields – relativity – dense matter – magnetic fields

1. Introduction

The question whether and, if so, how the magnetic field of isolated neutron stars (NSs) decays is a controversial issue and a subject of hot scientific debates. The observed rotational periods P and time derivative \dot{P} of about 700 pulsars (PSRs) (see PSR catalogue, Taylor et al. 1993) and studies of their inferred surface magnetic field strength versus their active age (τ_a) provide evidence that the magnetic fields of NSs is subject to decay.

This evidence is rather strong for the old population of PSRs, i.e. $\tau_a \gg 100$ Myrs, while for the younger population evidence for magnetic field decay is much weaker. As investigated by population synthesis methods (Bhattacharya et al. 1992, Hartman et al. 1997), observations and models are in harmony provided one accepts the hypothesis that NS magnetic field decays very little during the first $\tau_a \lesssim 10$ Myrs. The NS magnetic field decay depends strongly on where is the field located in the NS, what is its structure and strength. It is also related to the equation of state (EOS) of NS matter and the conductive properties of dense matter which are moreover affected by its thermal history too. In case the field is of fossil origin, or alternatively has been generated via a dynamo action during the proto-NS phase (Thompson & Duncan 1993), it is expected to thread most of the star. Early estimates of the electric conductivity of NS matter lead to the conclusion that magnetic field of NSs will not be dissipated during a Hubble time (Baym et al. 1969). However, more recent investigations regarding the conductive properties of nuclear matter in the presence of a strong B-field yield conductivities leading to much shorter field decay times (see e.g. Haensel et al. 1990, Goldreich & Reissenegger 1992, Urpin & Shalybkov 1995, Shalybkov & Urpin 1997). Besides the conductive properties of nuclear matter, another distinct mechanism leading to a B-decay process is based on the idea of magnetic flux expulsion from NS core driven by rotation or/and buoyancy (Muslimov & Tsygan 1985; Srinivasan et al. 1990). Once the expelled field reaches the star’s crust it subsequently suffers Ohmic decay. Ding et al. (1993) considered in detailed this process and have found typical decay times of the order of 100 Myrs. Recent investigations, which take into account the effect of the NS crust onto the process of flux expulsion (Konenkov & Geppert 2000) estimated even longer decay times for a field anchored in fluxoids in the superfluid NS core.

Although the issue of whether the field is penetrating the entire star or part of it is an open one, there exist, however, good reasons to believe that the NS magnetic field is maintained by currents in the crust. One possibility is the generation of the field via thermomagnetic effects during the first years of the NS life (Blandford et al. 1983, Urpin et al. 1986, Wiebicke & Geppert 1996). The most recent and detailed investigation of the magnetic and spin evolution of isolated NSs with a crustal dipolar

field has been performed by Urpin & Konenkov (1997, UK97 thereafter). They found a good agreement with observational data provided the EOS is not too soft, the initial surface magnetic field strength lies in the range of 10^{12} to 3×10^{13} G and is initially confined to densities of 10^{12} to 10^{13} g cm $^{-3}$ within the crust. Miralles et al. (1998) considered the effect of a crustal field decay onto the thermal evolution of a NS and they have concluded that a considerable amount of heating takes place in the the crust after about 3 to 10 Myrs, a period during which the NS has cooled down to $\lesssim 10^5$ K. Consequently, Joule heating can maintain a warm ($\approx 5 \cdot 10^4$ K) NS surface for a period of hundreds of Myrs.

All of the above described works ignore the curvature of spacetime. To date there exist no calculation treating self consistently the thermal and magnetic evolution of NSs which incorporate General Relativistic (GR) effects. As it has been argued elsewhere by the present authors (Geppert et al. 2000, referred to as GPZ00 hereafter), relativistic effects on the B-field evolution must be included in detailed investigations. A previous attempt to incorporate GR effects has been presented by Sengupta (1997, 1998). However this author apparently did not take into account the proper boundary condition associated with relativistic treatment and furthermore his formalism applies only to a Schwarzschild geometry. Moreover, he claims that the decay rate of the field is decreased by several orders of magnitude, a conclusion being in variance with the one obtain by GPZ00 and the present work.

In the present paper we investigate in details and in a self consistent manner, GR effects at first on both: the thermal and magnetic evolution of NSs. We consider three different EOSs and via numerical integration of Einstein's equations, neutron star models are constructed characterized by the compactness ratio varying in a large range. We solve simultaneously the relevant evolution equations and thus our approach naturally reveals the mutual dependencies of EOS, mass-to-radius relation, initial field structure and strength, and thermal history of NSs. In particular, as far as the cooling is concerned we consider two scenarios: the 'standard' slow neutrino emission scenario and also the so called enhanced neutrino emission which results in a much lower temperatures in young NSs. In order to avoid dealing with the uncertainties related to the behavior of the field within the superconducting core, as a first step in the present paper, we consider only magnetic fields not penetrating the NS core. Thus, the present analysis is within the framework of the crustal magnetic field hypothesis. We use our results from the GR treatment of thermal and magnetic field evolution implemented by a semi-relativistic treatment of the spin evolution to confront the crustal field hypothesis to observational data.

The paper is organized as follows: In the subsequent section we remind the reader of the GR formulation of the equations of stellar structure, the heat transport and conservation equations as well as the induction equation on a static spherically symmetric background geometry. We also present the evolution equations for an axisymmetric dipolar magnetic field as well as relativistic expressions for the Joule heating. Sect. 3 describes the microphysics used in our models. In Sect. 4 we present the

results of our model calculations and Sect. 5 is devoted to the discussion of the results. We briefly conclude in Sect. 6.

2. General relativistic formalism of static spherical stars

The spacetime geometry will be assumed to be spherically symmetric, which means that our results may not be accurate for fast rotating neutron stars. Employing the familiar Schwarzschild coordinates (t, r, θ, ϕ) , the interior and exterior spacetime geometry takes the form (Misner et al. 1973; Wald 1984)

$$ds^2 = -e^{2\Phi} c^2 dt^2 + \frac{dr^2}{1 - 2Gm/c^2r} + r^2 d\Omega^2. \quad (1)$$

The radial proper length is thus $dl = dr/\sqrt{1 - 2Gm/c^2r}$ and the proper time $d\tau = e^\Phi dt$.

Einstein's equations coupled to a perfect fluid energy-momentum tensor give us the standard equations (Misner et al. 1973; Wald 1984):

$$\frac{dm}{dr} = 4\pi r^2 \rho, \quad (2)$$

which determines the so called mass function $m = m(r)$,

$$\frac{d\Phi}{dr} = \frac{Gmc^2 + 4\pi Gr^3 P}{c^4 r^2 (1 - 2Gm/c^2r)}, \quad (3)$$

for the 'gravitational potential' $\Phi = \Phi(r)$ and the TOV equation of hydrostatic equilibrium

$$\frac{dP}{dr} = -(\rho c^2 + P) \frac{d\Phi}{dr} = -\frac{(\rho + P/c^2)(Gm + 4\pi Gr^3 P/c^2)}{r^2(1 - 2Gm/c^2r)}. \quad (4)$$

Regularity of the geometry at $r = 0$ implies the inner boundary condition for Eq. 2

$$m(r = 0) = 0 \quad (5)$$

while for Eq. 4 the central pressure

$$P(r = 0) = P_c \quad (6)$$

is specified, through the EOS of the form $P = P(\rho)$, with the central density ρ_c treated as a free parameter. Due to the linear nature of Eq. (3), Φ can be scaled so that it always can be arranged to fulfill:

$$e^{\Phi(R)} = \sqrt{1 - \frac{2GM}{c^2R}}, \quad (7)$$

Once the interior spacetime geometry has been so specified it is joined smoothly across the "surface" of the star to an exterior Schwarzschild field characterized by $M = m(R)$.

It should be mentioned that the stellar surface in our computation is fixed by

$$R = R_{\text{star}} = r(\rho = \rho_b) \quad (8)$$

where $\rho_b = 10^{10}$ g cm $^{-3}$. This guarantees that the EOS is temperature independent. The layers at densities below ρ_b , called the *envelope*, are treated separately (see Sect. 2.4).

2.1. Thermal evolution equations

Besides the above equations of stellar structure we shall need the equations describing the thermal evolution of the star. At the temperatures we are interested in, the neutrinos have a mean free path much larger than the radius of the star (Shapiro & Teukolsky 1983) and thus leave the star once they are produced. Energy balance arguments (see for instance Thorne 1966) then imply

$$\frac{d(Le^{2\Phi})}{dr} = -\frac{4\pi r^2 n e^\Phi}{\sqrt{1-2Gm/c^2r}} \left(\frac{d\epsilon}{dt} + e^\Phi (q_\nu - q_h) \right) \quad (9)$$

where L is the internal luminosity, ϵ the internal energy per baryon, q_ν, q_h is the neutrino emissivity and heating rate *per baryon* while n stands for the baryon number density. The corresponding inner boundary condition for L is

$$L(r=0) = 0 \quad (10)$$

The time derivative of ϵ can be written in the form

$$\frac{d\epsilon}{dt} = \frac{d\epsilon}{dT} \cdot \frac{dT}{dt} = c_v \cdot \frac{dT}{dt} \quad (11)$$

through the specific heat at constant volume c_v (which, for degenerate matter, is the same as the specific heat at constant pressure c_P).

The energy transport equation is :

$$\frac{d(Te^\Phi)}{dr} = -\frac{3}{16\sigma_{SB}} \frac{\kappa\rho}{T^3} \frac{Le^\Phi}{4\pi r^2 \sqrt{1-2Gm/c^2r}} \quad (12)$$

where T is the local temperature, σ_{SB} the Stefan-Boltzmann constant and κ the ‘opacity’. (Note that within the relativistic framework an ‘isothermal’ configuration is defined by $e^\Phi \cdot T = \text{constant}$ instead of $T = \text{constant}$.) The associated boundary condition is

$$T_b = T_b(L_b) \quad (13)$$

which relates the temperature at the outer boundary (defined more precisely further bellow), T_b , to the luminosity, L_b , in this layer. The location of this outer boundary layer is chosen such that L_b be equal to the total photon luminosity of the star, $L_* \equiv L(r=R)$, which in turn is related to the effective temperature T_e by $L_* \equiv 4\pi R^2 \sigma_{SB} T_e^4$. We can thus write Eq. 13 as $T_b = T_b(T_e)$ and this ‘ $T_b - T_e$ relationship’ is discussed in Sect. 2.4.

The opacity is related to the total (thermal) conductivity by:

$$\lambda = \frac{16\sigma_{SB} T^3}{3\kappa\rho}. \quad (14)$$

If one neglects the red-shift e^Φ and defines the energy flux F as $L/(4\pi r^2)$ one can write Eq. 12 as

$$F = -\lambda \cdot \nabla T \quad (15)$$

where ∇ is the radial gradient calculated with the proper length, which is the usual form of the heat conduction equation. The total conductivity is the sum of the electron and photon conductivities

$$\lambda = \lambda_e + \lambda_\gamma \quad (16)$$

since these two processes of heat conduction work independently and in parallel.

We will present our results of thermal evolution by using the ‘effective temperature at infinity’ $T_e^\infty \equiv T_e \cdot e^{\Phi(R)}$ related to the ‘luminosity at infinity’ $L_*^\infty \equiv L_* \cdot e^{2\Phi(R)}$ through the ‘radius at infinity’ $R^\infty \equiv R \cdot e^{-\Phi(R)}$ by

$$L_*^\infty = 4\pi(R^\infty)^2 \sigma_{SB}(T_e^\infty)^4. \quad (17)$$

These three quantities ‘at infinity’ are, in principle, measurable and, in particular, R^∞ would be the areal radius of the star that an observer ‘at infinity’ would measure with an extremely high angular resolution instrument (Page 1995).

The solution of the complete set of equations of stellar structure, Eqs. (2-7) and thermal evolution, Eqs. (9-13), requires knowledge of the equation of state, the opacity κ , the neutrino emissivity q_ν and also the specific heat c_v . We shall devote Sect. 3 to the detailed specification of those variables.

2.2. Magnetic evolution equations

Besides the equations of stellar structure and thermal evolution we shall also need the equations describing the magnetic field evolution. In this paper consideration will be restricted to dipolar (poloidal) magnetic fields. The GR formulation of the evolution equation of such fields has been discussed in detail by GPZ00 while for a more general set up see Rädler et al. (2000). As has been shown in the first reference, such a field can be expressed in terms of a relativistic generalization of the familiar Stokes stream function (see, e.g., Moffatt 1978, page 53) by:

$$B^r(t, r, \theta) = \frac{2F(t, r)}{r^2} \cos \theta, \quad (18)$$

$$B^\theta(t, r, \theta) = -\frac{1}{r} \left(1 - \frac{2Gm}{c^2 r} \right)^{\frac{1}{2}} \frac{\partial F(t, r)}{\partial r} \sin \theta. \quad (19)$$

while the relevant induction equation (see Appendix) yields the following equation for the relativistic Stokes function

$$\begin{aligned} \frac{4\pi\sigma}{c^2} e^{-\Phi} \frac{\partial F}{\partial t} &= \left(1 - \frac{2Gm}{c^2 r} \right) \frac{\partial^2 F}{\partial r^2} \\ &+ \frac{1}{r^2} \frac{\partial F}{\partial r} \left[\frac{2Gm}{c^2} + \frac{4\pi G}{c^2} r^3 \left(\frac{P}{c^2} - \rho \right) \right] - \frac{2}{r^2} F. \end{aligned} \quad (20)$$

The appropriate boundary conditions, as $r \rightarrow 0$, is the same as in the flat space case: a regular field at the star’s center requires $\frac{F(t, r)}{r^2}$ to be finite. The outer boundary condition, however, differs from that valid in the flat space, and its GR form is as follows (see GPZ00):

$$R \left. \frac{\partial F(t, r)}{\partial r} \right|_R = G(y) F(t, R) \quad (21)$$

where:

$$G(y) = y \frac{2y \ln(1-y^{-1}) + \frac{2y-1}{y-1}}{y^2 \ln(1-y^{-1}) + y + \frac{1}{2}} \quad \text{with } y = R/R_S \quad (22)$$

($R_S \equiv 2GM/c^2$ being the star's Schwarzschild radius). Since $G(y) < 0$ (in particular, in the flat space-time case, $G(\infty) = -1$) the boundary condition forces a bending of F in the upper layers.

As an initial profile for the Stokes function we use the same formula as UK97, for later comparison with the work of these authors:

$$F(r, 0) = B_0 R^2 (1 - r^2/r_0^2)/(1 - R^2/r_0^2) \quad \text{at } r > r_0 \quad (23)$$

$$F(r, 0) = 0 \quad \text{at } r < r_0$$

Note that this initial $F(r, 0)$ does not satisfy the outer boundary condition, but will immediately be forced to do it at the first numerical time step. There will thus be a rapid relaxation of F in its early evolution due to the enforcement of the boundary condition and the propagation of the resulting curvature of F toward higher densities.

2.3. Joule heating

Due to the finite conductivity σ , magnetic energy is dissipated into heat (= Joule heating). The heat production per unit (proper) time and unit (proper) volume is given by

$$Q_h = n \cdot q_h = \frac{j^2}{\sigma} \quad (24)$$

where j is the current. As it is shown in the Appendix, for a dipole poloidal magnetic field B , j is given by $j = j_\phi e_\phi$ with

$$j_\phi = \frac{c \sin \theta}{4\pi r} \times \left\{ e^{-\Phi} \left(1 - \frac{2Gm}{c^2 r}\right)^{\frac{1}{2}} \frac{\partial}{\partial r} \left[e^{\Phi} \left(1 - \frac{2Gm}{c^2 r}\right)^{\frac{1}{2}} \frac{\partial F}{\partial r} \right] - \frac{2F}{r^2} \right\}. \quad (25)$$

It is seen immediately that in the limit $e^\Phi = 1$ and $m = 0$ the above expression reduces to its flat space-time counterpart (Miralles et al. 1998). Since our numerical calculations assume spherical symmetry we use, in Eq. 25, a spherical average of $\sin^2 \theta$ ($\langle \sin^2 \theta \rangle = \frac{2}{3}$) obtaining

$$\langle Q_h \rangle = \frac{c^2}{24\pi^2} \frac{1}{\sigma} \frac{1}{r^2} \times \left\{ e^{-\Phi} \left(1 - \frac{2Gm}{c^2 r}\right)^{\frac{1}{2}} \frac{\partial}{\partial r} \left[e^{\Phi} \left(1 - \frac{2Gm}{c^2 r}\right)^{\frac{1}{2}} \frac{\partial F}{\partial r} \right] - \frac{2F}{r^2} \right\}^2. \quad (26)$$

2.4. Outer boundary: magnetized envelopes

The layers at densities below $\rho_b = 10^{10} \text{ g cm}^{-3}$ are defined as the *envelope*, and extend up to the *atmosphere*, where the *photosphere* is located, while by *interior* we mean the whole star where $\rho > \rho_b$. The presence of the magnetic field affects strongly the heat transport in the envelope (but not in the deeper layer where $\rho > 10^{10} \text{ g cm}^{-3}$, which motivates the above choice of ρ_b), and results in a non uniform distribution of the surface

temperature. The corresponding ' $T_b - T_e$ relationships' have been calculated by Page & Sarmiento (1996) for dipolar (and quadrupolar) fields. We use these results which hence give us a field dependent ' $T_b - T_e$ relationship' that adjust itself to the evolution of the magnetic field. Note however that, for fields much stronger than 10^{12} G , this relationship is not reliable when T_e is much lower than 10^6 K , and it is most probably very inaccurate when T_e is below 10^5 K .

Our outer boundary condition assumes that the envelope is made of catalyzed matter. If an upper layer of light elements were present, the heat transport is strongly enhanced when no magnetic field is present (Potekhin et al. 1997), but there is, to date, no published model of magnetized envelopes with light elements.

One should finally emphasize that when the thermal evolution is controlled by the Joule heating the star's luminosity, and T_e , is given by the heating rate and is independent of the outer boundary condition as discussed at the end of Sect. 4.2.

This closes the system of equations and boundary conditions to be solved.

2.5. Numerical method

The thermal evolution equations are solved by a Henyey-type code (e.g., Page 1989) while the induction equation for the Stokes function is solved with a Crank-Nicholson method (Press et al., 1986). The whole set of equations for the thermo-magnetic evolution should be solved simultaneously at each time step but we have decided to solve the thermal and then the magnetic equations alternatively, i.e., the thermal equations are solved at a given time step using the field of the previous step (which appears in the Joule heating term) and once the new temperature is obtained the induction equation is solved to obtain the new magnetic field. This method is much faster than a full simultaneous solution and gives results which, as we have verified explicitly in a few case, are practically indistinguishable from the full simultaneous solution.

3. Input microphysics

3.1. The equation of state

The first ingredient needed to build NS models is the equation of state (EOS). In principle the EOS should give us not only the relationship between pressure and density, i.e., $P = P(\rho)$, but also the chemical composition of matter.

We separate the crust from the core at the density $\rho = \rho_{cr} \equiv 1.6 \times 10^{14} \text{ g cm}^{-3}$ (Lorenz et al. 1993) and use the EOSs of Negele & Vautherin (1973) for the inner crust, at $\rho > \rho_{drip} \equiv 4.4 \times 10^{11} \text{ g cm}^{-3}$, and Haensel et al. (1989) for the outer crust, i.e., we assume that the chemical composition is that of cold catalyzed matter. The EOS, and its associated chemical composition, in the crust is well determined under the assumption that matter is in its (catalyzed) ground state. There is however still the possibility that a strong phase of hypercritical accretion occurred after the supernova explosion, which may, or may not, alter the chemical composition of the crust. We will

Table 1. Properties of the $1.4 M_{\odot}$ neutron star models

EOS	Radius [km]	Crust thickness [km]	Crust mass [M_{\odot}]	Central density [10^{15} g/cm^3]	Moment of inertia [10^{45} g cm^2]
Stiff	14.94	1.52	0.069	0.49	1.83
Medium	10.48	0.72	0.022	1.17	1.08
Soft	7.1	0.22	0.003	5.59	0.72

not consider this possibility here but only mention that it does have an enormous effect on the magnetic field and its subsequent evolution (Geppert et al. 1999a)

In the core, the EOS is relatively well constrained up to densities around $2\text{--}3 \times \rho_{cr}$ while its behavior at higher densities is still a mystery (Prakash 1998). Since we only study magnetic fields confined to the crust, the details of the core's structure are not important to us, except for the neutrino emission and pairing which strongly affect the cooling and are separately described below. The most relevant property of the high density EOS, for our purpose, is that it determines the size of the star and, hence, the thickness of the crust. We will thus consider three different cases which hopefully illustrate the whole range of possibilities. We take as a 'Medium EOS' the one calculated by Wiringa et al. (1988), using their model called av14+UVII, a 'Stiff EOS' from Pandharipande, Pines & Smith (1976) and a 'Soft EOS' from Pandharipande (1971). Note that the Stiff EOS is based on the presence of a lattice of neutrons in the inner core and is not anymore considered as realistic but we still use it since it has been used by many authors and represents the case of extreme stiffness. Moreover, none of the consequences of the presence of such a lattice phase is taken into account in our calculations, e.g., in C_v , ϵ_ν and the transport coefficients: we will assume that neutrons and protons form a quantum liquid and also boldly consider them as superfluid and superconductor. Our opinion is that this EOS should be abandoned but we consider it for comparison with previous works of other authors. The Soft EOS on the other hand, includes hyperons and is also based on outdated microphysics but is nevertheless still representative of modern soft EOSs for our concerns and represents the case of extreme softness. Again, we use this particular soft EOS to facilitate comparison with the work of previous authors (who often dubbed it as the 'BPS EOS').

We will consider models of $1.4 M_{\odot}$ stars whose overall properties are listed in Table 1.

3.2. Neutrino processes

Neutrino emission drives the cooling as long as the internal temperature is higher than about 10^8 K. For processes in the crust we consider the two dominant ones which are the plasmon process and the electron-ion bremsstrahlung (Page 1989). The former is only relevant during the first few years of the life of the NS but is very strong and brings down the crust temperature to about 10^9 K, relaxing it from the arbitrary initial conditions.

The latter has only a very small effect, mostly when the surface temperature is around 10^6 K, i.e., for young stars.

The crucial neutrino emission processes occur in the core and we consider two scenarios (see Page 1998 for more details). In the 'Standard Cooling', or 'slow cooling', scenario we include the modified Urca processes and their associated, and weaker, bremsstrahlung processes following Yakovlev & Levenfish (1995). This scenario applies when the NS core contains only neutrons, protons, as well as electrons and muons which maintain charge neutrality, and the proton fraction is low enough that the direct Urca process is forbidden by momentum conservation. In the 'Enhanced Cooling', or 'fast cooling', cases we add a strong neutrino emission at densities larger than $\rho_{fast} = 4 \times 10^{14} \text{ g cm}^{-3}$ with a rate

$$\epsilon_\nu^{FAST} = 10^{26} (\rho/\rho_{cr})^{2/3} T_9^6 \text{ erg g}^{-1} \text{ s}^{-1} \quad (27)$$

where $T_9 \equiv T/10^9$ K. This rate is representative of many of the possible enhanced ones as the direct Urca from nucleons or hyperons, but is stronger than what produced by a pion or kaon condensate (Prakash 1998). For comparison, the inefficient modified Urca process gives approximately $\epsilon_\nu^{MURCA} \sim 10^{21} T_9^8 \text{ erg g}^{-1} \text{ s}^{-1}$.

In our three model $1.4 M_{\odot}$ stars, the masses of the inner cores where the fast neutrino emission is allowed for the 'Enhanced Cooling' cases are, 0.11, 1.29 and $1.39 M_{\odot}$ for the Stiff, Medium and Soft EOS, respectively.

3.3. Pairing

The occurrence of pairing, neutron superfluidity and proton superconductivity, strongly affects both the thermal and magnetic evolution of neutron stars. The thermal effects are very strong during the neutrino cooling phase, which last from about 10^5 to almost 10^7 yrs depending on the model, and the subsequent photon cooling phase (see, e.g., Page 1998 for a review). As a result, pairing will in a large part determine the time at which Joule heating starts to control the thermal evolution but then, during this Joule heating phase, the effect of pairing becomes negligible. We treat the suppressive effect of pairing on C_v and ϵ_ν according to the treatment of Levenfish & Yakovlev (1994a, 1994b) and Yakovlev & Levenfish (1995).

The superconductive phase in the core has the effect of producing an impenetrable barrier for the magnetic field, which is initially confined to the crust in the models of the present work. This guarantees the confinement of the magnetic field, and the currents, to the crust since the superconductive phase transition happens, at the crust-core boundary, well before the magnetic field had time to diffuse to this layer. For definiteness, we plot in Fig. 1 the pairing critical temperatures that we adopt in this paper. The values we adopt for $^1\text{S}_0$ pairing of both neutrons and protons are typical of modern calculations. In the case of neutron $^3\text{P}_2$ pairing we explicitly adopt values which vanish at densities above $10^{15} \text{ g cm}^{-3}$ to ensure that pairing will not suppress the strong neutrino emission in our Enhanced Cooling scenarios for the Soft and Medium EOSs.

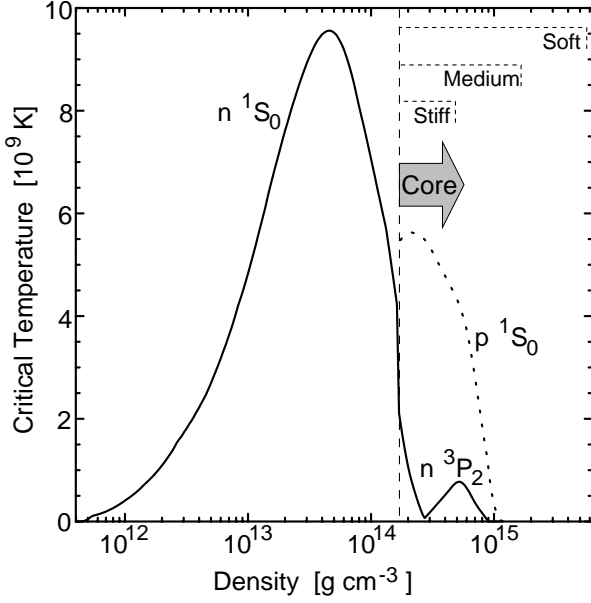


Fig. 1. Pairing critical temperatures adopted in this work, for neutrons in the 1S_0 state (from Ainsworth et al. 1989) and 3P_2 state (from Takatsuka 1972) and protons in the 1S_0 state (from Baldo et al. 1992). The short dash lines show the central densities of our three model $1.4 M_\odot$ stars with the Soft, Medium and Stiff EOS.

In the case of the Stiff EOS any published calculation of neutron or proton pairing shows a non vanishing value of T_c at the density in the center of the star, given the low value of this central density. To avoid suppression of the neutrino emission by pairing we will assume that *the fast neutrino emission is not affected by neutron and proton pairing in this case of Stiff EOS in the Enhanced Cooling scenario.*

3.4. Electrical conductivities

In general, the electrical conductivity σ can be expressed in terms of the electron relaxation time τ as

$$\sigma = \frac{e^2 n_e \tau}{m_e^*}, \quad (28)$$

where

$$m_e^* = \mu_e / c^2 = m_e [1 + 1.018 (\rho_6 Z/A)^{2/3}]^{1/2} \quad (29)$$

is the electron effective mass and n_e the electron number density (μ_e being the electron chemical potential, $\rho_6 = \rho/10^6 \text{ g cm}^{-3}$, Z and A the charge and mass number of the ions). In the liquid phase we use the calculation of $\tau = \tau_{e-i}$ for electron-ion scattering by Itoh et al. (1983). In the solid phase τ is given by

$$\frac{1}{\tau} = \frac{1}{\tau_{e-ph}} + \frac{1}{\tau_{e-imp}} \quad (30)$$

where we use the results of Itoh et al. (1984) for the electron-phonon scattering τ_{e-ph} and of Yakovlev & Urpin (1980) for the electron-impurity scattering τ_{e-imp} . In general, τ_{e-i} is a function of ρ , A and Z , and τ_{e-ph} depends also on the temperature T while τ_{e-imp} depends on ρ , Z and the impurity concentration

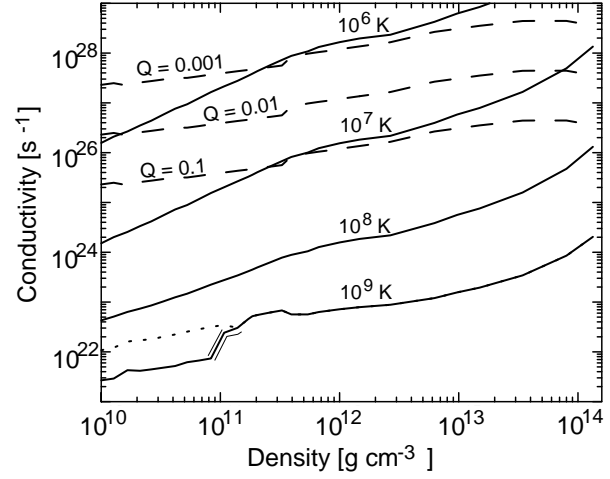


Fig. 2. Electrical conductivities in the crust. The dashed lines show σ_{imp} , which is temperature independent, for three different values of the impurity content Q_{imp} . The continuous lines show σ for electron-phonon scattering, in the solid phase, and electron-ion scattering, in the liquid phase, at four different temperatures. Note that these four curves all correspond to the solid phase except for the 10^9 K one where the low density part is still in the liquid phase: the dotted extension show the value σ would have if the matter were in the solid phase and the short tripped segment indicates the region where σ is interpolated between the electron-phonon and the electron-ion values. Finally, the increase of σ in this 10^9 K case at densities just above the transition density, i.e., temperatures just below the melting temperature, is due to the Debye-Waller factor (Itoh et al. 1984). For comparison with the cooling curves, notice that interior temperatures of 10^6 , 10^7 , 10^8 , and 10^9 K roughly correspond to effective temperatures around 10^5 , 3×10^5 , 10^6 , and 3×10^6 , respectively.

Table 2. Initial magnetic field configurations and impurity concentrations in our three classes of models.

Model	B_0 [G]	ρ_0 [gm/cm ³]	Q_{imp}
1	10^{11}	10^{12}	0.1
2	10^{12}	10^{13}	0.01
3	10^{13}	10^{14}	0.001

Q_{imp} . We show in Fig. 2 the value of σ for typical values of T and Q_{imp} .

4. Results

We will present here our results for the thermal, magnetic and rotational evolution of isolated neutron stars considering $1.4 M_\odot$ stars built with the three EOSs described above within both the ‘standard’ and the ‘fast’ cooling scenarios. In order to investigate the influence of the (a priori unknown) initial structure and strength of the magnetic field onto NS’s evolution, we considered for each EOS and cooling scenario three classes of qualitatively different field models, existent at the beginning of the evolution. They are characterized by the initial surface field strength B_0 , depth of penetration of the current ρ_0 and impurity concentration Q_{imp} as listed in Table 2.

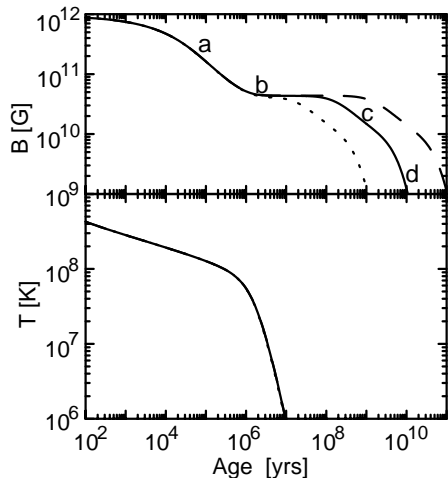


Fig. 3. Evolution of the internal temperature (lower panel) and surface magnetic field for the model described in Fig. 4, continuous line. The two models in dashed and dotted lines show the corresponding evolution for impurity contents $Q_{\text{imp}} = 0.001$ and 0.1 , respectively (the continuous line has $Q_{\text{imp}} = 0.01$). Note that in these cases the heating is so small that the three models follow the same thermal evolution track.

4.1. A detailed example

We first discuss here an example of the internal evolution of the Stokes function, magnetic field, currents and local heating rate, as shown in Fig. 4, which will help for the general discussion presented below. We choose the $1.4 M_{\odot}$ star with the medium EOS and ‘standard’ cooling; the initial surface field strength is 10^{12} G and the currents are initially located at $\rho_0 = 10^{13}$ g cm $^{-3}$. The impurity content for σ_{imp} is $Q_{\text{imp}} = 0.01$. This is the model 2 of the central panel of Fig. 5 but it is reproduced in Fig. 3 along with two similar models with different impurity contents (upper panel) and the evolution of the internal temperature (lower panel). Note that at the plotted times the star has practically reached isothermality. GR effects are included but will be discussed in the next subsections.

The four chosen times, labeled as a, b, c & d are marked in the upper panel of Fig. 3 and correspond, respectively, to a) the initial field decay during the period when the neutron star is still hot and σ is temperature dependent, being dominated by electron-phonon scattering, b) the plateau where the cooling lead to an enormous increase of σ , and consequently a stagnation of the field decay, which will eventually be controlled by impurity scattering, c) second phase of decay of the field when time becomes comparable to the impurity scattering decay time scale and, finally, d) the late exponential decay.

The four panels of Fig. 4 directly illustrate the diffusion of the field toward regions of higher conductivity as time runs. Once σ becomes T independent the diffusion equation formulates an eigenvalue problem whose solution can be formally written as $F(\rho, t) = \sum_{n=1}^{\infty} \exp(-t/\tau_n) a_n F_n(\rho)$, in terms of eigenmodes F_n with decay times τ_n , and expansion coefficients a_n . Since the n -th mode, $F_n(\rho)$, has n nodes, in the crust, initially a very large number of modes must contribute signifi-

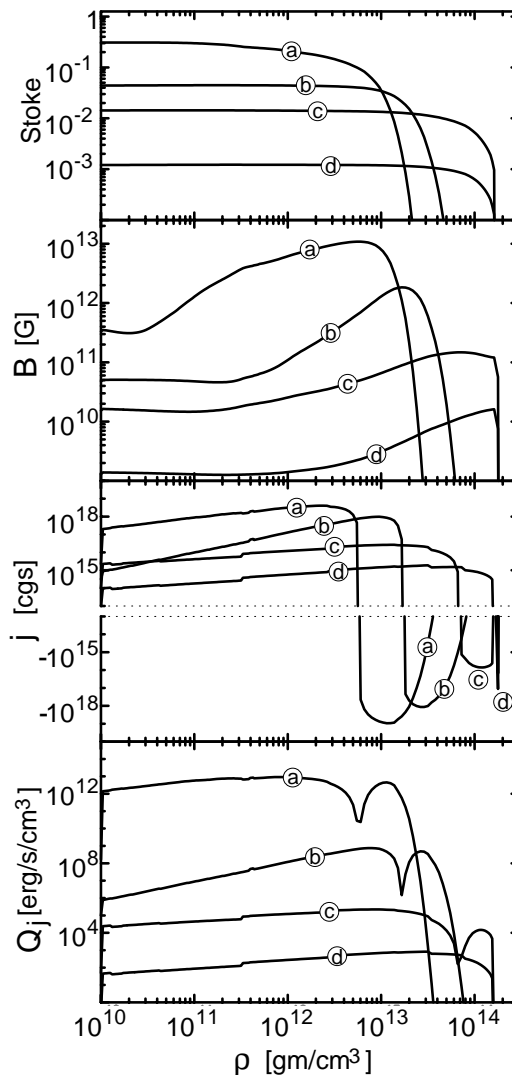


Fig. 4. Stokes function, magnetic field, B , currents, j , and Joule heating rate, Q_j in the crust, for model 2 of the central panel of Fig. 5. See text, Sect. 4.1, for details.

cantly, i.e., with large positive and negative coefficients a_n , to produce a mutual cancellation resulting in a vanishing $F(\rho, t)$ in the high density region. The diffusion of the stoke function into the high density region is simply due to the faster decay of the modes with $n > 1$ compared to the nodeless fundamental mode. When the fundamental mode is dominating, i.e., when the stoke function is non zero in the whole crust (it has reached the crust-core boundary through diffusion), the field evolution is a power-law like decay, phase c (Urpin et al. 1994). Finally, when only the fundamental mode $n = 1$ is left the decay becomes purely exponential, phase d.

Note that the field strength inside the crust is at least one order of magnitude higher than at the surface: this is due to a very large B_{θ} forced by the presence of the derivative dF/dr in Eq. 19, while at the surface the boundary condition ensures that B_r and B_{θ} are comparable.

With respect to the currents, noticeable are the negative currents in the layers where the field is growing which are due to induction, i.e., Lenz law. Once the field has reached the crust-core boundary the currents are positive in the whole crust and the only negative currents left are the supercurrents induced in the skin layer of the proton superconductor. Instead of imposing an ad-hoc boundary condition at the crust-core interface to simulate the effect of the proton superconductor we have preferred to keep the central boundary condition and introduce an enormous value for σ , 10^{200} s^{-1} , once protons become superconductor, i.e., when $T < T_c$. This allows us to see explicitly the induced supercurrents which, however, because of the finite radial resolution of the numerical scheme, are located in the whole last zone of the crust instead of the physical skin layer of the superconductor which is a few tens of fermis thick. We have checked explicitly that an ad-hoc crust-core boundary condition for F gives the same results as our boundary condition with enormous σ .

As a last remark, from Fig. 3, and comparing with Fig. 2, we see that impurity scattering starts to dominate σ after the field has reached the plateau (phase b): this stagnation value of the field is independent of Q_{imp} and is only a result of the enormous increase of σ due to the cooling. After this, the length of the plateau (phase b) is controlled by Q_{imp} , higher impurity contents leading naturally to an earlier onset of the second phase of field decay (phase c).

4.2. Magneto-thermal evolution within the ‘standard’ cooling scenario

In Figs. 5 and 6 we present the modeled evolution of the, more or less, observable quantities, i.e. the surface temperature (measured by a far distant observer) and the surface magnetic field. While the surface temperatures, or, at least, its upper limits, of isolated NSs can be inferred from X–ray spectra, the magnetic field of isolated pulsars is mostly estimated by the precise measurement of the rotational period and its time derivative.

Within the ‘standard’ cooling scenario the surface temperature stays quite high ($\sim 10^6 \text{ K}$) during the neutrino dominated cooling era, which lasts about $\sim 10^6 \text{ yrs}$ (for our Stiff EOS models) to almost $\sim 10^7 \text{ yrs}$ (Soft EOS models). Later on the cooling is driven by photon emission from NS’s surface which appears in the cooling curves as a strong increase in the slope. During the neutrino cooling era, the surface temperature drops by a factor of about 2 (Stiff EOS) to 4 (Soft EOS), i.e. the approximately isothermal crust has at the end of the neutrino cooling epoch a temperature of about $5 \cdot 10^7$ (Soft EOS) to 10^8 K (Stiff EOS). As seen from Fig. 2, for such and higher temperatures, the electrical conductivity in the crust is determined by electron–phonon collisions except at the highest densities. With the following temperature drop during the photon cooling era, the electron–phonon relaxation time $\tau_{e\text{-ph}}$ increase dramatically and thus impurity scattering will begin to control σ (see Eq. 30), at a temperature, and thus an age, depending on the impurity concentration. From that stage on, σ becomes temperature independent.

Note that the differences in the thermal evolution for the different EOSs, before Joule heating becomes efficient, are mostly due to the differences in the fraction of the core which is paired. A larger paired region implies a lower neutrino emission, and thus a higher temperature during the neutrino cooling era, and also a lower specific heat, and thus an earlier transition to the photon cooling era and a faster temperature drop during that era (see, e.g., Page 1998). We have taken here the choice of well defined density dependences of T_c , for both the neutrons and protons, independently of the EOS, as shown in Fig. 1. Different density dependences of the T_c ’s would obviously give different results. For example, assuming high values of T_c down to center of the star for the Soft EOS would result in a cooling history practically indistinguishable from the cooling history of the Stiff EOS model. Given the present uncertainty on the value and density dependence of T_c for ${}^3\text{P}_2$ neutron pairing (Baldo et al. 1998) any choice has, unfortunately, some arbitrariness. Any effect of the resulting cooling history on the field evolution should thus be specifically formulated in terms of cooling history and not in terms of the stiffness of the EOS.

We have, very roughly, for the field decay time-scale, $\tau_{\text{decay}} \propto l^2$, l being a typical length scale of the crustal field structure. This immediately implies that τ_{decay} increases when ρ_0 increases and also when the stiffness of the EOS is increased, since both increase l . Moreover, since also $\tau_{\text{decay}} \propto \sigma$, a higher ρ_0 locates the currents in a region of higher σ and increases more τ_{decay} . Thus, the models 1 give fast decay, models 2 intermediate decay and models 3 slow decay, as is clear from Fig. 5.

The cooling influences the field decay by rising σ till it becomes temperature independent when dominated by impurity scattering. This happens during the photon cooling era as mentioned above, and happens earlier for stiffer EOSs *given our choice of EOS independent T_c ’s*. Consequently, we obtain that a stiffer EOS results in a slower field decay because of its cooling behavior and also because of the larger length scale l . Our choice of T_c thus maximalize the effect of the EOS’s stiffness on the field decay.

We now turn our discussion to the analysis of GR effects upon magnetic field evolution. For each model we simulated the field evolution with and without GR effects, but note that GR effects on the star structure and cooling have always included. (Had we, for instance, turned off the GR effects on the star structure, the resulting models would make no sense at all since the changes in the size, the central density etc, of the model would render them unrealistic.) On the other hand, GR effects on the cooling have already been discussed in the literature long ago (Nomoto & Tsuruta 1987, Gudmundsson et al. 1983). The models with GR effects included are marked as ‘GR’ in Fig. 5 and drawn with thick lines. It is seen from those plots that the decay of the field is faster in NSs built on the Soft EOS than in the case of the Medium or Stiff EOS but the decelerating GR effects are more pronounced. This is most remarkable for long living fields: the difference of the surface field strength for model 3, with the Soft EOS, after 10^{10} yrs of evolution is about four orders of magnitude. Comparing the field evolution for the Soft and Stiff EOS cases, while the final surface field

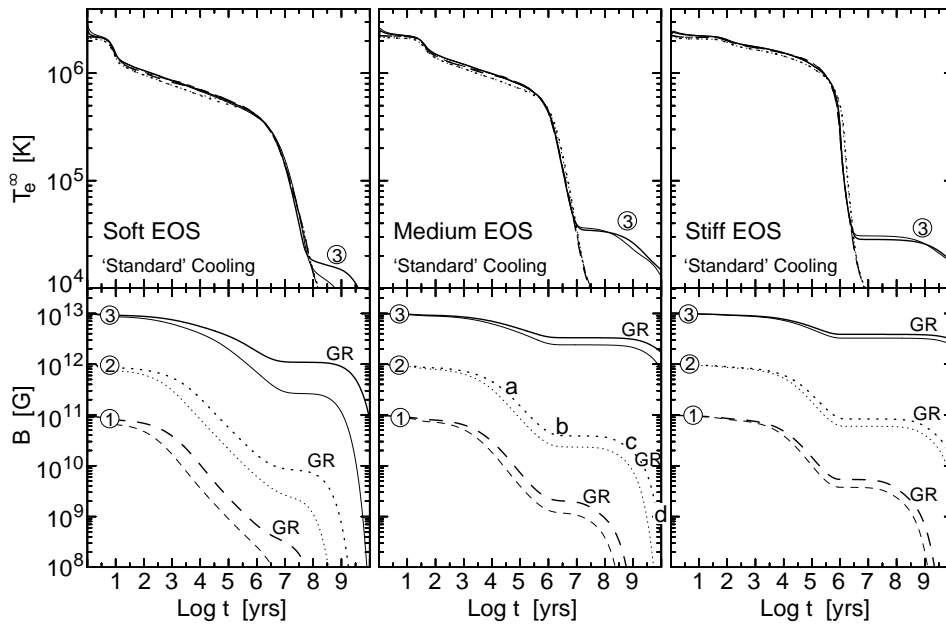


Fig. 5. Thermal and magnetic evolution within the ‘standard’ cooling scenario. Evolutionary curves are labeled following notations of Table 2. See text, Sect. 4.2, for details.

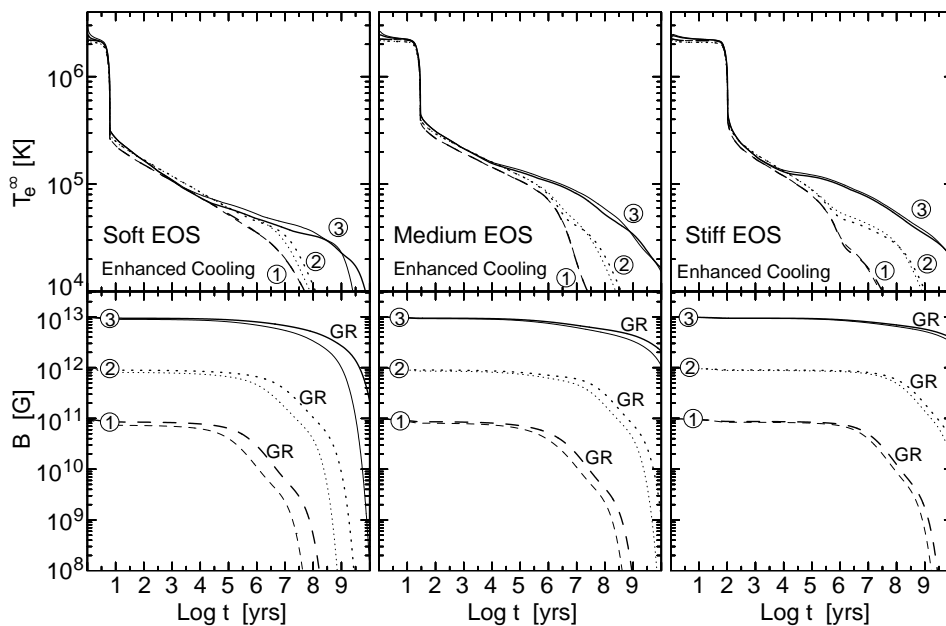


Fig. 6. Cooling and field evolution within the ‘fast’ cooling scenario. Evolutionary curves are labeled following notations of Table 2. See text for details.

strength for model 3 in the Stiff case is larger than that of the Soft case by a factor of 10^5 when GR effects are neglected, that factor reduces to about 50 when relativistic effects are taken into account correctly.

In the late photon cooling era, when most of the initial thermal energy of the NS has been irradiated away, the Joule heating by the decay of the crustal field completely determines the cooling behavior. Note, however, that most of the magnetic energy has been dissipated earlier when it had no effect on the cooling. The amount of heat released in the process of Joule heating is determined by the strength of the field at that time and its decay rate. Therefore, an initial field configuration as given by models of class 3 will result in a significant Joule heating while in models of class 1 the effect is practically nil. The field decay of the class 2 models yields some noticeable Joule heating only in

case of the Stiff EOS since its strength is large enough for that until about 10^8 yrs. For long periods Joule heating is especially effective in NSs with a stiff EOS: their crust is quite thick, they keep a larger field and there is a lot of magnetic energy to dissipate. The effect of GR on the Joule heating is not spectacular but still noticeable in the case of a soft EOS at the latest stages. For the different EOSs it can result in stronger or weaker heating: the rate of dissipation of magnetic energy is lower with GR but the magnetic energy to be dissipated is larger due to the previous slower evolution and the net effect can be an enhancement or a reduction of the heating.

Note that at these late ages when the thermal evolution is entirely controlled by the Joule heating the outer boundary condition, Eq. 13, has no influence on the thermal evolution: this is due to the fact that the heating mechanism is temperature inde-

pendent since σ is totally controlled by impurity scattering. The star's luminosity L_* is thus simply given by the total heating rate integrated over the whole star

$$L_*^\infty = H \equiv \int q_h e^{2\Phi} dV \quad (31)$$

since, given the low temperature at this times, $q_\nu \ll q_h$. This is very fortunate for our study since the ' $T_b - T_e$ relationship' is poorly known at the low temperatures reached in this late phase of evolution. This would of course not be the case if the heating mechanism were temperature dependent.

Let us mention that, in the case of magnetars, the Joule heating dominates the cooling from the very beginning and thus has a strong effect onto the field evolution (Geppert et al. 1999b).

With the field strengths we consider in this work, the field affects the thermal evolution at times when the conductivity is temperature independent and there is thus no feedback of the field strength on the field decay. Consequently, the field evolution depends linearly on B_0 and the evolution curves of Fig. 5 can be scaled up or down, a fact we will use in Sect. 4.4.

4.3. Magneto-thermal evolution within the 'fast' cooling scenario

Enhanced neutrino emission is caused by the presence of 'exotic' states of matter in the NS core. Kaon or pion condensation, hyperons, quarks as well as possible direct Urca processes enormously enlarge the neutrino emissivity. This results in a very fast cooling of the core, so that during the so called *isothermalization phase* the heat of the hotter crust is transported into the core. Depending on the EOS and the assumptions about pairing that phase can last of the order of 1 to 100 yrs (see, e.g., Page 1998). During this phase the surface temperature drops very rapidly and after this the crustal temperature is so low that the conductivity is almost completely controlled by electron-impurity collisions. Thus, for a period of time given by the impurity decay time scale τ_{imp} , the field suffers practically no decay. For $t > \tau_{\text{imp}}$ the field decays according to a power law and, when it has diffused down to the crust-core boundary, the decay becomes exponential. In class 3 models the power law like decay is missed because the field is already initially located close to the crust-core boundary so that it reaches this depth during τ_{imp} . Note that $\tau_{\text{imp}} \propto Q_{\text{imp}}^{-1}$ and that it is also reduced with the softening of the EOS as an effect of the decreasing crustal thickness. Generally, the field decay is slower than in the 'standard' cooling scenario.

Due to the accelerated cooling, the Joule heating, even for the model 1 and 2 fields, dominates the cooling earlier compared to the 'standard' cooling scenario. At ages above $\sim 10^7 - 10^8$ yrs, however, the star's temperature is comparable, or even higher, to that predicted by the analogous models within the 'standard' cooling scenario. In class 2 and particularly class 3 models with the Stiff EOS, the stars' temperatures in this range of ages are noticeably higher, compared to the analogous 'standard' cooling cases, since the magnetic field is higher and thus the joule heating more efficient. After 10^{10} yrs, however, the

difference in the surface temperatures between the 'standard' and the accelerated cooling scenario vanishes.

As in the case of 'standard' cooling, the field evolution scales linearly with its initial value B_0 .

4.4. Rotational evolution

Given the temporal evolution of the magnetic field for the various EOSs and cooling scenarios, the rotational period of the NSs can be estimated by integrating the equation which relates the loss of rotational energy to the radiation of electromagnetic energy by magneto-dipole radiation

$$P \dot{P} = \frac{2\pi^2}{3} \frac{R^6 \tilde{B}^2(t)}{cI}, \quad (32)$$

where \tilde{B} is surface magnetic field at the magnetic pole, and I is the star's moment of inertia. An accurate relativistic expression for the moment of inertia is given by $I = 0.21 e^{-2\Phi} MR^2$ (Ravenhall & Pethick 1994). However, this classical magneto-dipole radiation formula assumes flat space-time. Ideally we would like to have the exact GR version of this equation. To our knowledge, the GR version of it remains to be calculated and in the absence of the exact formula we shall only use an approximate expression. We may recall that Eq. 32 implicitly considers the energy loss at the light cylinder and then extrapolates the field strength back to the star's surface assuming the flat space-time $1/r^3$ radial dependence of the field. The full GR solution of a slowly rotating dipolar field, in vacuum, shows however (Muslimov & Tsygan 1990, 1992) that the actual field at the star's magnetic pole is amplified by a factor $f = -3y^2[y \ln(1 - y^{-1}) + \frac{1}{2}(2 + y^{-1})]$, where $y \equiv R/R_S$, compared to the flat space-time one. For instance, for our Soft EOS star of $1.4 M_\odot$, the resulting value of the amplification factor is $f = 1.86$ while for the Stiff one, $f = 1.27$ (Page & Sarmiento 1996). In view of the Muslimov-Tsygan results, we will henceforth relate the surface magnetic field B at magnetic pole as we numerically calculated it, to the corresponding field \tilde{B} used in Eq. 32 for the rotational evolution by $B = f \tilde{B}$. For each of our three EOS (and a fixed stellar mass of $1.4 M_\odot$) and the two cooling scenarios, we specify the initial field strength and current depths ρ_0 and finally the impurity content Q_{imp} . The specification of those parameters yields a unique evolution for the surface B -field and via Eq. 32 the corresponding P . The resulting magneto-rotational evolution of isolated NSs is presented in Fig. 7.

We have also plotted, as dots, the PSRs data of the Princeton catalogue (Taylor et al. 1993): their B field is calculated with Eq. 32, using P and \dot{P} from that catalogue and the appropriate GR ' f factor' for each stellar model. The star's radius R and moment of inertia I correspond to the values of the respective models of mass $1.4 M_\odot$ for each of our EOSs. The set of B - P diagrams of Fig. 7 is the arena where our theoretical models confront reality. There is a major effect on the data interpretation arising from varying the EOS: we see that given the observed P - \dot{P} data the "observed" surface B -field of pulsars differ almost one order of magnitude when we consider models where

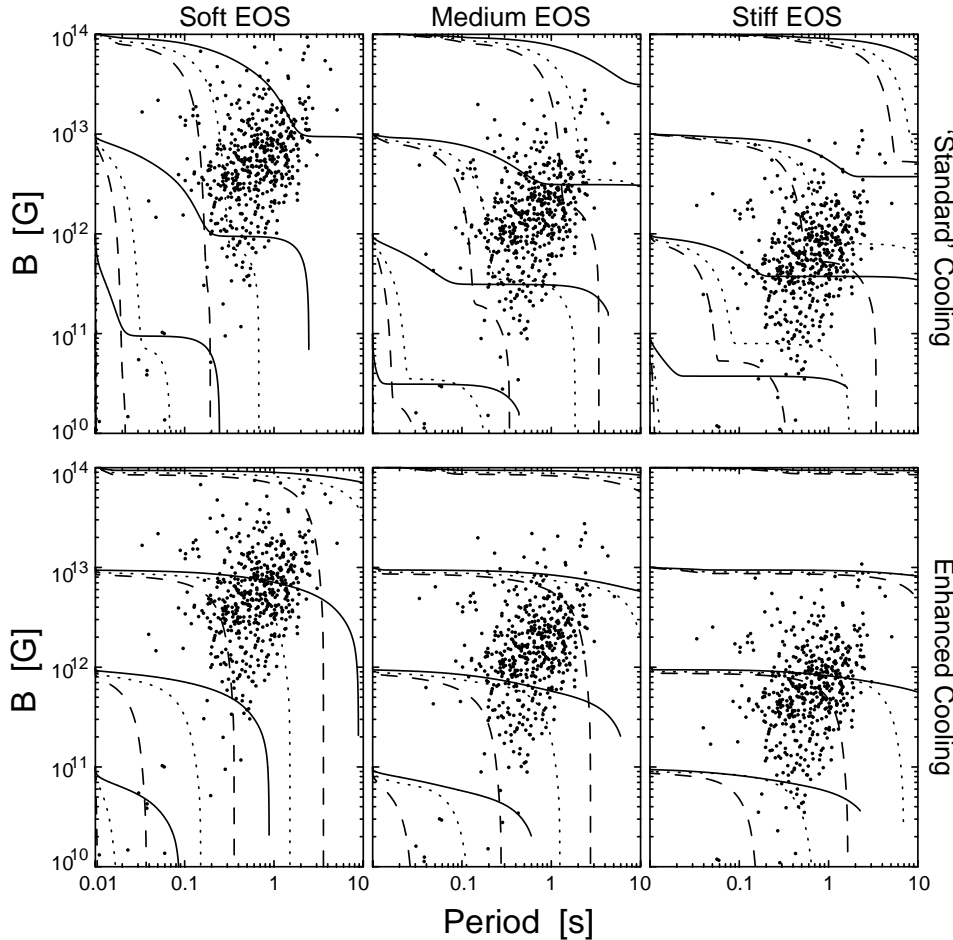


Fig. 7. Predicted magneto-rotational evolution of pulsars. The field evolutions come from the results of Fig. 5 and 6 scaled to various initial B_0 . Continuous lines correspond to initial current locations and impurity contents of $(\rho_0, Q_{\text{imp}}) = (10^{14} \text{ g cm}^{-3}, 0.001)$, dotted lines to $(\rho_0, Q_{\text{imp}}) = (10^{13} \text{ g cm}^{-3}, 0.01)$, and dashed lines to $(\rho_0, Q_{\text{imp}}) = (10^{12} \text{ g cm}^{-3}, 0.1)$. For each EOS, cooling scenario and initial field strength these three evolutionary tracks range from the most slowly decaying field (continuous curve) to the fastest decaying field (dashed curve) and thus encompass the whole range of predictions for the dynamical evolution of a neutron star with a crustal field.

the equation of state is varied from the extreme soft one up to the extreme stiff one (see also UK97). This effect is a straightforward consequence of the fast growth of the magnetic field at small distance from the star, which is moreover amplified by GR effects, combined with the much smaller stellar radius obtained by employing the Soft EOS. It should be emphasized however, that although a complete and accurate model of pulsar spin-down will probably alter the simple Eq. 32 (expected at least to modify the overall numerical coefficient) it certainly will not change the radial dependence of the field in the near zone.

A basic feature emerging from the Fig. 7, is the following: a given model is viable if it manages to maintain a strong enough field for a long enough time such that its rotational period can increase up to values compatible with the bulk of the observed pulsar population. It is also clear that if a ‘standard’ cooling scenario applies and irrespectively of the EOS, the field decays much faster than in the case of the accelerated cooling: this results in smaller saturation values of the rotational periods compared to the accelerated cooling model, with the same initial field structure and the same EOS.

The evolutionary tracks offer the possibility to check whether a given EOS can be naturally compatible with the observational constraints without extreme “fine tuning” of the initial parameters ρ_0 and B_0 , of the impurity parameter Q_{imp} and its preference to standard versus enhanced cooling. Thus, for in-

stance: assuming a soft EOS, a comparison of the evolutionary tracks with the observed pulsar population strongly favors the enhanced cooling scenario. Within the ‘standard’ cooling scenario, only the strongest initial fields $\sim 10^{14}$ G are acceptable. In this case, even $B_0 \sim 10^{13}$ G requires very high ρ_0 and very low Q_{imp} , definitely making the ‘standard’ cooling scenario with a soft EOS very unappealing. Note that the fast cooling scenario is very natural for a soft EOS since the central densities reached in NSs are above ten times nuclear matter density. Even if the pulsar fields (for a given P) were much lower than estimated we would still be in the same situation since the high field is required to spin down the pulsars to the range of observed P ’s before the field decays too much. In the case of a medium EOS the requirements are much less stringent. Within the ‘standard’ cooling scenario, initial fields of the order of 10^{12} G require high initial depths ρ_0 and low pollution in order for the evolutionary tracks to reach the bulk of the pulsar population. Finally, in the case of a stiff EOS, the field decay is slow enough that the whole pulsar population is reachable with initial fields in the range $10^{11} - 10^{13}$ G without basically any significant restrictions on ρ_0 and Q_{imp} in both the fast and the slow cooling scenarios.

One cannot overemphasize that the above analysis is plagued by the intrinsic uncertainties of Eq. 32 and should be considered as only indicative. Moreover, it is worth stressing

here that tracks starting with an initial field $B_0 = 10^{14}$ G have to be considered with reserve since for such (and larger) field strengths the decay may not any longer described by a linear diffusion equation. The possible occurrence of a Hall-cascade (Goldreich & Reissenegger 1992) would imply that the field evolution would deviate significantly from Eq. 20, which is strictly valid in the limit that the magnetization parameter $\omega_B \tau < 1$ (ω_B being the Larmor frequency and τ the relaxation time of the electrons as given by Eq. 30).

5. Discussion

We studied in detail, and for a large variety of possible models, the magnetic, thermal, and rotational evolution of isolated NSs, assuming that their magnetic fields, and the currents supporting them, are confined to the stellar crust. Our calculations take into account, for the first time, all mutual effects of the thermal and magnetic evolution self consistently in a wholly GR formalism.

5.1. Comparison with the work of Urpin and Konenkov

Urpin & Konenkov (1997, UK97 thereafter) have presented the most detailed study of the evolution of crustal neutron star magnetic field while Miralles et al. (1998) completed the former work by the inclusion of Joule heating in the thermal evolution. It should be mentioned, however, that neither of these works incorporated GR effects on the B -field evolution.

Our field evolution results, without GR effects incorporated, are very close to those of UK97 (their curves labeled 3, dashed lines, in their Fig. 2 correspond to our models 2). The main differences are seen in the early evolution of the field (our phase a): this can be easily attributed to the fact that UK97 started the field evolution at an age of 100 yrs while we started it immediately at the star's birth. Since UK97 used isothermal stars for their modeling of the B -field evolution they could not model the early hot, and non isothermal, phase properly. In our calculations, this time difference allows the initial currents to rapidly relax from their initial distribution (Eq. 23, which *does not* fulfill the outer condition condition) during a phase of low conductivity while the models of UK97 must do it in conditions of higher conductivity, i.e., their relaxation is much slower. However, if one contemplates the scenario in which crustal magnetic fields are generated by a thermomagnetic instability during this early hot phase (Blandford et al. 1983, Urpin et al. 1986, Wiebicke & Geppert 1996) it is equally reasonable to start the B -field evolution by pure ohmic decay at the end of this phase as UK97 did. The slight differences seen in the strength of the field at the onset of the impurity scattering dominated phase (phase b) can be easily explained as due to slight differences in the cooling histories, particularly differences in the time at which photon cooling takes over neutrino cooling (the knee at ages around $10^6 - 10^7$ yrs) and also as a result of the differences in the previous phase a.

Finally, the field evolution in the late phases, c and d, agree well with the results of UK97 once we take into account the small differences in the previous phases.

5.2. General relativistic effects

While previous studies considered the influence of GR effects into the star's structure and on its thermal evolutions (see e.g. Page 1989), their incorporation into the magnetic field evolution had not been properly accounted for. In the present paper we have been working with the GR version of the diffusion equation, Eq. 20, accompanied by proper boundary conditions, Eq. 21, derived in detail by GPZ00.

The analysis of GPZ00 clearly showed that most of the effect of GR on the field decay is due to the presence of the red-shift factor e^Φ in Eq. 20. This can be intuitively understood by noticing that the red-shift factor relates the proper time in each layer inside the star, i.e., the physical time in the layer where the currents are located and decaying, to the time of an observer who is observing the decay, at infinity (i.e., the coordinate time). As it can be easily seen from Eq. 20, the effects of the red shift factor on the field decay could be approximated by a flat space-time diffusion equation running however on a slower time scale, given by some kind of averaged red-shift. This is clear from our Figs. 5 and 6 where the GR curves have the same shape as the non-GR ones but shifted to the right.

Comparing the field evolution when GR effects are included with the evolution when they are neglected, we see that we obtain quite larger fields already in phase a, and in the late decay (phase c), we obtain much larger fields, by up to four orders of magnitude for very compact stars. GR effects in a field evolution can be viewed as almost equivalent to an evolution without GR effects but with currents initially located to higher densities and, in the late decay phase, with lower impurity content. This means that all constraints previously obtained about the location of the currents and the impurity contents of the crust are significantly weakened when GR effect are taken into account.

5.3. Comparison with the work of Sengupta

As far as the previously mentioned work of Sengupta (1998) is concerned, although we are in qualitative agreement with his results, we find many quantitative as well as interpretational differences. For instance this author considered a soft EOS (similar to the one we used) and field configurations with currents supposedly initially located at densities of 2×10^{11} and 4×10^{11} g cm $^{-3}$. However, we obtain much higher densities at the depths at which he locates these layers: using his values of $x \equiv r/R = 0.979$ and 0.9834 we find densities of the order of 6×10^{13} and 2.6×10^{13} g cm $^{-3}$ respectively. Consequently, his field decay curves should be compared with our class 2 models: we see then a rough quantitative agreement with respect to the importance of the GR effects with the significant difference that the late exponential decay (phase d) is absent in his GR models. As mentioned above, since the B -field evolutionary curves with and without GR effects should show approximately similar shapes we deduce that the different behavior of the B field at late times obtained by Sengupta, must be mostly due to numerical inaccuracies possibly combined with his neglect of

appropriate boundary conditions at the stellar surface as well as his employment of the Schwarzschild geometry.

5.4. Constraining the neutron star EOS and cooling history within the crustal magnetic field hypothesis

The analysis of the $B - P$ diagrams of Sect. 4.4 may be a tool to constrain the structure of matter at high density. In a similar analysis, UK97 concluded that a stiff EOS with ‘standard’ cooling is the most promising model for understanding the observed pulsar population properties and that a medium EOS requires currents located at relatively high densities and low impurity contents. These authors prefer the ‘standard’ cooling scenario on the basis that it implies an early decay of the field which may have an observational support in the fact the young pulsars with an associated supernova remnant have stronger magnetic field than the bulk of the population. Our results, with GR included, show that a medium EOS with ‘standard’ cooling is also compatible with the observed P and \dot{P} with much weaker constraints on the initial dipole strength B_0 and penetration density ρ_0 and on the impurity content Q_{imp} than when GR effects are neglected. A soft EOS with ‘standard’ cooling needs very special conditions to accommodate the observational data: very large B_0 , high ρ_0 , and very low Q_{imp} .

But, notice that in case fast neutrino cooling is operating any EOS could be compatible with the observed pulsar population with only weak constraints on B_0 , ρ_0 , and Q_{imp} as we argued in Sect. 4.4. However, this cooling scenario is more physical in the case of a soft EOS and probably incompatible with an EOS as stiff as our Stiff EOS (for which the central density of a $1.4 M_\odot$ star does not even reach twice the nuclear density). In summary, it appears rather difficult within the crustal field hypothesis alone to draw any strong conclusion about the EOS of neutron stars and their cooling histories.

5.5. The EOS and cooling history of neutron stars and the crustal magnetic field hypothesis

There exist independent arguments in favor of a not too soft neutron star EOS, none of them being, at the present time, compelling. Interpretation of kilohertz quasi-periodic oscillations (KHz QPO’s) in several low mass X-ray binaries indicate these systems contain neutron stars with masses around $2 M_\odot$ (Kluźniak 1998) which a very soft EOS is not able to sustain. The strong gravitational light bending around a very compact star would make it almost impossible for such a star to show any modulation in its surface thermal emission, in contradiction to some observations (Page & Sarmiento 1996).

With regard to the thermal evolution of neutron stars, comparison of cooling models with current estimate of surface temperature of young neutron stars shows no clear evidence of occurrence of fast cooling (Ögelman 1995; Page 1998). This means that if these neutron stars do contain some ‘exotic’ phase of matter, its strong neutrino emission must be quenched by pairing (Page & Applegate 1992; Page 1998) so that their thermal evolution is very close to the ‘standard’ one.

These two lines of arguments are consistent with the conclusions arising from the crustal field hypothesis, including GR effects: the EOS of neutron stars is away from the very soft regime and their thermal evolution is close to the prediction of the ‘standard’ model.

5.6. Joule heating and detectability of old isolated neutron stars

Our study of the effect of the Joule heating produced by the decaying currents gives results very similar to the ones of Miralles et al. (1998) and shows that the GR effects on the field evolution do not introduce any important change on the resulting late time thermal evolution.

Another consequence of the GR effects on the B-field evolution is that we can predict significantly stronger field strength over a Hubble time. This implies that Old Isolated Neutron Stars will be spinning very slowly and are hence more likely to be able to accrete matter from the interstellar medium. As a consequence, this significantly increases the chances of detecting them through their thermal radiation, either due to the Joule heating or to the accretion.

6. Conclusions

The effect of GR on both the thermal and magnetic evolution is to slow it down, mostly because the proper time inside the star runs more slowly than the observer’s time. This effect is of course stronger the more compact the star is. On the other hand, with increasing compactness the field decay, as any diffusion process, is accelerated because of the reduction of the length scale. The competition of these two opposite tendencies reduces the sensitivity of the field evolution to the softness or stiffness of the EOS. As a result, it is difficult to draw conclusions about the nature of the dense matter EOS from magnetic field evolution studies alone. However when taking into account information from other approaches, as the cooling history, gravitational lensing, kHz QPO’s, a consistent picture of neutron star structure and evolution is obtained, in which the EOS is not too soft and the cooling history is close to the so called ‘standard’ cooling scenario.

Reversely, we can consider these results as an argument in favor of the crustal magnetic field hypothesis. It is seen to be compatible with the observed distribution of pulsars in the $P-\dot{P}$ diagram without requiring fine tuning of the models’ parameters. Moreover, these model parameters are consistent with values deduced from various other neutron star studies.

Acknowledgements. This work was supported by a binational grant DFG (grant #444 - MEX - 1131410) - Conacyt (grant #E130.443), Conacyt (grant #2127P - E9507), UNAM - DGAPA (grant #IN105495) and Coordinación Científica - UMSNH. D.P. and T.Z. are thankful to the Astrophysikalisches Institut Potsdam for its kind hospitality and U.G. to the Instituto de Astronomía of UNAM.

Appendix A: induction equation and joule heating rate

In this appendix, we shall provide a few of the intermediate calculations leading to the derivation of the relativistic expression for the Joule heating employed in the numerical computations. We begin by recalling that the covariant form of Maxwell's equations are as follows (Misner et al. 1973; Wald 1984):

$$\nabla^\alpha F_{\alpha\beta} = -\frac{4\pi}{c} J_\beta \quad (\text{A.1})$$

$$\nabla_{[\alpha} F_{\beta\gamma]} = 0 \quad (\text{A.2})$$

where $F_{\alpha\beta} = -F_{\beta\alpha}$, J_α and ∇ are the coordinate components of the Maxwell tensor, the conserved four current and the covariant derivative operator, respectively. We may first recall that once a solution $F_{\alpha\beta}$ of Eqs. A.1–A.2 has been specified, an observer with four velocity U^α , $U^\alpha U_\alpha = -1$ measures electric and magnetic fields (\mathbf{E} , \mathbf{B}) given, respectively, by:

$$E_\alpha = F_{\alpha\beta} U^\beta, \quad B_\alpha = -\frac{1}{2} \epsilon_{\alpha\beta\gamma\delta} F_{\gamma\delta} U^\beta \quad (\text{A.3})$$

where $\epsilon_{\alpha\beta\gamma\delta}$ stands for the four-dimensional Levi-Civita tensor density. It follows then easily from Eq. A.3 that an inversion yields:

$$F_{\alpha\beta} = U_\alpha E_\beta - U_\beta E_\alpha + \epsilon_{\alpha\beta\gamma\delta} U^\gamma B^\delta \quad (\text{A.4})$$

Thorne et al. (1982, 1986) have introduced an elegant version of curved spacetime electrodynamics, the absolute space formulation, that is reminiscent of the familiar flat spacetime electrodynamics formulated in terms of the electric and magnetic fields. This can be accomplished by working directly with the physical frame components of the electric and magnetic fields (\mathbf{E} , \mathbf{B}), as determined by the static observers relative to their orthonormal frames. Recalling that such observers have a four velocity field $U^a = e^\Phi \delta_o^a$, (see Eq. 1) it then follows that Maxwell's Eqs. A.1–A.2 can be written in the following equivalent form:

$$\nabla \cdot \mathbf{E} = 4\pi\rho, \quad \nabla \cdot \mathbf{B} = 0 \quad (\text{A.5})$$

$$\nabla \times (Z\mathbf{B}) = \frac{4\pi}{c} Z\mathbf{J} + \frac{1}{c} \frac{\partial \mathbf{E}}{\partial t} \quad (\text{A.6})$$

$$\nabla \times (Z\mathbf{E}) = -\frac{1}{c} \frac{\partial \mathbf{B}}{\partial t} \quad (\text{A.7})$$

where in this appendix Z stands for the lapse function related to the red shift factor by $Z = e^\Phi$ and the ∇ operators are formed out of the following three metric:

$$ds^2_3 = \frac{dr^2}{1 - 2Gm/c^2 r} + r^2 d\Omega^2. \quad (\text{A.8})$$

by the rules of vector calculus as applied to the above orthogonal coordinate system. It follows then rather easily that in the absence of any convective motion Eqs. A.5–A.7, combined with Ohm's law $\mathbf{J} = \sigma \mathbf{E}$, and within the MHD approximation (i.e., neglecting the displacement current in Eq. A.6), yield the following induction equation governing the evolution of the neutron star magnetic field:

$$\frac{1}{c} \frac{\partial \mathbf{B}}{\partial t} + \nabla \times \left[\frac{c}{4\pi\sigma} \nabla \times (Z\mathbf{B}) \right] = 0, \quad (\text{A.9})$$

The above form of the induction equation combined with Eq. A.8 as well the line element Eq. 1 with the metric functions corresponding to a non singular perfect fluid solution of Einstein's equations yield Eq. 20 of the main text (for a detailed derivation see GPZ00).

We now consider the GR expression for the Joule heating. To do so, we start from the covariant expression of the energy momentum tensor for an arbitrary electromagnetic field (Misner et al. 1973; Wald 1984) i.e.:

$$T_{\mu\nu} = \frac{1}{4\pi} \left[F_{\mu\gamma} F_{\nu}{}^\gamma - \frac{1}{4} g_{\mu\nu} F_{\alpha\beta} F^{\alpha\beta} \right]. \quad (\text{A.10})$$

Using the representation of Eq. A.4, one can easily show that the electromagnetic energy density \mathcal{E} as seen by the static observers is given by:

$$T_{\mu\nu} U^\mu U^\nu = \frac{1}{8\pi} [E^\alpha E_\alpha + B^\alpha B_\alpha] = \frac{1}{8\pi} [\mathbf{E} \cdot \mathbf{E} + \mathbf{B} \cdot \mathbf{B}] \equiv \mathcal{E} \quad (\text{A.11})$$

where \mathbf{E} and \mathbf{B} stand for the physical components of the electric and magnetic fields, respectively, satisfying Eqs. A.5–A.7. Poynting's theorem now has the following form

$$\frac{\partial \mathcal{E}}{\partial \tau} = -\nabla \cdot \mathbf{S} + 2\mathbf{g} \cdot \mathbf{S} - \mathbf{j} \cdot \mathbf{E} \quad (\text{A.12})$$

where

$$\mathbf{S} \equiv \frac{c}{4\pi} (\mathbf{E} \times \mathbf{B}) \quad (\text{A.13})$$

is the Poynting vector and

$$\mathbf{g} \equiv -\frac{\nabla Z}{Z} = -\nabla \Phi \quad (\text{A.14})$$

is the gravitational acceleration, $d\tau \equiv Z dt$ being the proper time interval. The second term in the r.h.s. of Eq. A.12 is a purely relativistic effect which results from the inertia of (electromagnetic) energy (see, e.g., Thorne et al. 1986). The only dissipative term in Eq. A.12 is the last one, i.e., the Joule heating term, using Ohm's law:

$$Q_h^{(\text{GR})} = \frac{\mathbf{j} \cdot \mathbf{j}}{\sigma} \quad (\text{A.15})$$

By construction $Q_h^{(\text{GR})}$ represents energy per unit (proper) time and (proper) volume.

References

- Ainsworth T.L., Wambach J., Pines D., 1989, Phys. Lett. B222, 173
 Baldo M., Cugnon J., Lejeune A., Lombardo U., 1992, Nucl. Phys. A536, 349
 Baldo M., Elgarøy Ø, Engvik L., Hjorth-Jensen M., Schultze H.-J., 1998, Phys. Rev. C58, 1921
 Baym G., Pethick C., Pines D., 1969, Nat 224, 673
 Bhattacharya D., Wijers R., Hartman J., Verbunt F., 1992, A&A 254, 198

- Blandford R.D., Applegate J.H., Hernquist L., 1983, *MNRAS* 204, 1025
- Ding K.Y., Cheng K.S., Chau H.F., 1993 *ApJ* 408, 167
- Geppert U., Page D., Zannias T., 1999a, *A&A* 345, 847
- Geppert U., Page D., Colpi M., Zannias T., 1999b, In: Kramer M., Wex W., Wielebinski R. (eds.) *Pulsar Astronomy – 2000 and Beyond*. ASP Conference Series
- Geppert U., Page D., Zannias T., 2000, *Phys. Rev. D*, in press (GPZ00)
- Goldreich P., Reisenegger A., 1992, *ApJ* 395, 250
- Gudmundsson E.I., Pethick D.J., Epstein R.I., 1983, *ApJ* 202, 286
- Haensel P., Urpin V.A., Yakovlev D.G., 1990, *A&A* 229, 133
- Haensel P., Zdunik J.L., Dobaczewski J., 1989, *A&A* 222, 353
- Hartman J., Bhattacharya D., Wijers R., Verbunt F., 1997, *A&A* 322, 477
- Itoh N., Kohyama Y., Matsumoto N., Seki M., 1984, *ApJ* 285, 758; erratum, *ApJ* 404, 418
- Itoh N., Mitake S., Iyetomi H., Ichimaru S., 1983, *ApJ* 273, 774
- Kluźniak W., 1998, *ApJ* 509, L37
- Konenkov D., Geppert U., 2000, *MNRAS* 313, 66
- Levenfish K.P., Yakovlev D.G., 1994a, *Astron. Lett.* 20, 54
- Levenfish K.P., Yakovlev D.G., 1994b, *Astron. Rep.* 71, 282
- Lorenz C.P., Ravenhall D.G., Pethick C.J., 1993, *Phys. Rev. Lett* 70, 379
- Miralles J.A., Urpin V., Konenkov D., 1998, *ApJ* 503, 368
- Misner C., Thorne K., Wheeler J.A., 1973, *Gravitation*. Freeman, San Francisco
- Moffatt H.K., 1978, *Magnetic Field Generation in Electrically Conducting Fluids*. Cambridge University Press, Cambridge
- Muslimov A.G., Tsygan A.I., 1985, *Ap&SS* 115, 43
- Muslimov A.G., Tsygan A.I., 1990, *SvA* 34, 133
- Muslimov A.G., Tsygan A.I., 1992, *MNRAS* 255, 61
- Negele J.W., Vautherin D., 1973, *Nucl. Phys.* A207, 298
- Nomoto K., Tsuruta S., 1987, *ApJ* 312, 711
- Ögelman H.B., 1995, In: Alpar M.A., Kiziloğlu Ü., van Paradijs J. (eds.) *The Lives of Neutron Stars*. Kluwer Academic Publishers, p. 101
- Page D., 1989, Ph.D. Thesis, SUNY Stony Brook
- Page D., 1995, *ApJ* 442, 273
- Page D., 1998, In: Alpar A., Bucccheri R., van Paradijs J. (eds.) *The Many Faces of Neutron Stars*. Kluwer Academic Publishers, p. 539
- Page D., Applegate J.H., 1992, *ApJ* 394, L17
- Page D., Sarmiento A., 1996, *ApJ* 473, 1067
- Pandharipande V.R., 1971, *Nucl. Phys.* A178, 123
- Pandharipande V.R., Pines D., Smith R.A., 1976, *ApJ* 208, 550
- Potekhin A.Y., Chabrier G., Yakovlev D.G., 1997, *A&A* 323, 413
- Prakash M., 1998, In: Hirsch J.G., Page D. (eds.) *Nuclear and Particle Astrophysics*. Cambridge University Press, Cambridge, p. 153
- Press, W.H., Flannery B.P., Teukolsky S.A., Vetterling W.T., 1986, *Numerical Recipes*. Cambridge University Press, Cambridge
- Rädler K.-H., Fuchs H., Geppert U., Rheinhardt M., Zannias T., 2000, in preparation
- Ravenhall D.G., Pethick C.J., 1994, *ApJ* 424, 846
- Sengupta S., 1997, *ApJ* 479, L133
- Sengupta S., 1998, *ApJ* 501, 793
- Shalybkov D., Urpin V., 1997, *A&A* 321, 685
- Shapiro S.L., Teukolsky S.A., 1983, *Black Holes, White Dwarfs, and Neutron Stars*. John Wiley & Sons, New York
- Srinivasan G., Bhattacharya D., Muslimov A.G., Tsygan A.I., 1990, *Current Sci.* 59, 31
- Takatsuka T., 1972, *Prog. Theor. Phys.* 47, 1062
- Taylor J.H., Manchester R.N., Lyne A.G., 1993, *ApJS* 88, 529
- Thorne K., 1966, *High Energy Astrophysics*. Gordon Breach, New York
- Thorne K., Macdonald D., 1982, *MNRAS* 198, 339
- Thorne K., Price R.H., Macdonald D.A., 1986, *The Membrane Paradigm*. Yale Univ. Press
- Thompson Ch., Duncan R.C., 1993, *ApJ* 408, 194
- Urpin V.A., Chanmugan G., Sang Y., 1994, *ApJ* 433, 780
- Urpin V., Konenkov D., 1997, *MNRAS* 292, 167 (UK97)
- Urpin V., Levshakov S., Yakovlev D., 1986, *MNRAS* 219, 703
- Urpin V., Shalybkov D., 1995 *A&A* 294, 117
- Wiebicke H.-J., Geppert U., 1996, *A&A* 309, 203
- Wald R.M., *General Relativity*. 1984, Chicago University Press, Chicago
- Wiringa R.B., Fiks V., Fabrocini A., 1988, *Phys. Rev.* C38, 1010
- Yakovlev D.G., Levenfish K.P., 1995, *A&A* 297, 717
- Yakovlev D.G., Urpin V., 1980, *SvA* 24, 303